Measurement: Sensors xxx (xxxx) xxx

Contents lists available at ScienceDirect

Measurement: Sensors

journal homepage: www.sciencedirect.com/journal/measurement-sensors

Development of a proximity contactless ammeter based on GMR sensors for measuring direct currents

ARTICLE INFO

Keywords:
GMR
Giant magnetoresistance
Magnetometer
Contactless ammeter

ABSTRACT

Conventional ammeters are inserted in series with the element in which the current is to be measured, constituting an invasive measurement form. Clamp ammeters measure non-invasively but are limited to alternating currents. For continuous currents measurements, Hall-based clamp ammeters are used, with low output voltages and little stability to temperature. Also, the need to involve the conductor in a magnetic core makes it impractical for some situations. This manuscript describes a proximity contactless ammeter based on giant magnetoresistance sensors capable of measuring direct currents some centimeters away from the conductor, non-invasively and with high resolution. Sixty tests were performed, with currents varying from −3 A to 3 A, with steps of 0.1 A. The prototype was able to estimate the current with type A expanded uncertainties of 100 mA and 0.19 cm for the distance. The results demonstrate the feasibility of conducting contactless current measurements using GMR sensors.

1. Introduction

Ammeters are instruments widely used in the electrical industry and service sectors, whose purpose is to measure the intensity of the electric current flowing through a conductor. Conventionally, the ammeter needs to be inserted in series with the element in which it is desired to measure the current, thus constituting an invasive measurement, which sometimes might be impractical since not always a circuit can be easily alterable. This is also the case of the shunt ammeter, which has its functioning based on Ohm's Law. Another complication is that the insertion of the shunt changes the current to be measured [1,2].

Non-invasive measurement of electrical current is possible and solves such disadvantages. An electric current passing through a straight conductor generates a circular magnetic field around it, whose intensity varies with the current intensity [1,2]. Among the ammeters based on this principle, which use coil type sensors, clamp ammeters are traditionally used in applications for measuring alternating currents, by positioning a coil around the electric conductor which, when traversed by an alternating current, will produce an alternating magnetic field. The electric current can be calculated due to a direct proportionality between the current intensity and the resulting voltage at the coil terminals (induced by the magnetic field according to Faraday's law), and it is possible to estimate the electric current [1,2].

For the measurement of continuous currents, however, there is no induction of electric current in the coil, as the circumferential magnetic field is continuous. In this case, it is necessary to directly measure the magnetic field, and associate its magnitude with the intensity of the primary electric current. A usual magnetic field transducer in this application is the Hall effect sensor. When subjected to an external magnetic field, this sensor generates a voltage proportional to this field and, with a suitable conversion, it is possible to determine the current that runs through the conductor [1,2]. Over the past years, several research groups have developed different alternatives for the contactless measurement of electrical current, as briefly described below.

Sánchez et al. [3] designed an ammeter for laboratory purposes based on a giant magnetoresistive (GMR) spin-valve sensor capable of measuring direct currents up to ±10 A with a very small experimental deviation from the reference of ±30 mA (0.3 %). However, the experimental setup is very application-specific, with the conductor having a U-shape with two GMR sensors placed in the opposite legs, all integrated in a PCB board. In fact, it is similar to a conventional ammeter, with the current being measured passing through the measuring instrument, so it is not comparable to the prototype herein presented.

Pai et al. [4] developed a power sensor for smart grid applications, the current measurement being based in an inductive sensor (solenoid) capable of measuring currents from 0.1 A to 10 A with a 1.3 mm distance between the wire and the surface of the solenoid. The results indicate errors between 2 % and 4 %, but the small distances involved make it unpractical for several situations.

Xiaoguang et al. [5] designed a current sensor based on a giant magnetoresistance (GMR) sensor and a toroid magnetic core for wide applications prospects that need high precision current sensing in high frequency. The results demonstrate that the current sensor has a linear error lower than ±0.7 %, can measure frequencies up to 100 kHz and has high linearity in the 10 mA to 20 A range. However, the measuring scheme is similar to a clamp Hall ammeter, with the conductor passing through a magnetic ring where the magnetometer is placed, thus hindering its application in situations where it is not possible to access the vicinity of the conductor (e.g. a conductor attached to a wall or embedded into it).

Yong et al. [6] presented a practical contactless current sensor based on magnetic tunnel junction (MTJ) sensors for smart grid applications

https://doi.org/10.1016/j.measen.2024.101444

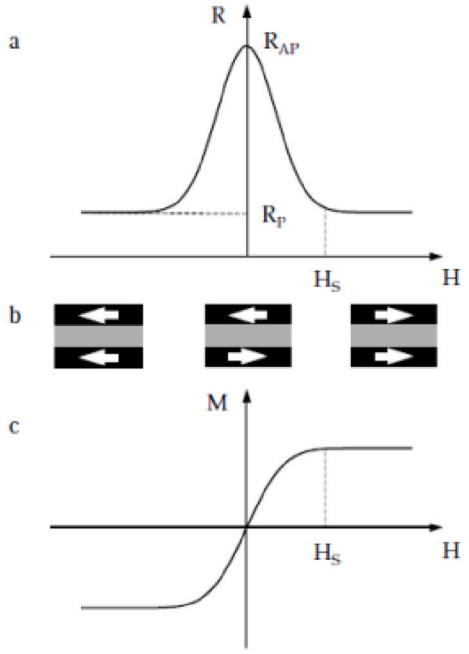

Fig. 1. Schematic representation of the GMR effect. (a) Variation of the resistance of a magnetic multilayer as a function of the applied field. (b) Magnetization settings (indicated by the arrows) on the multilayer. (c) Magnetization curve [11].

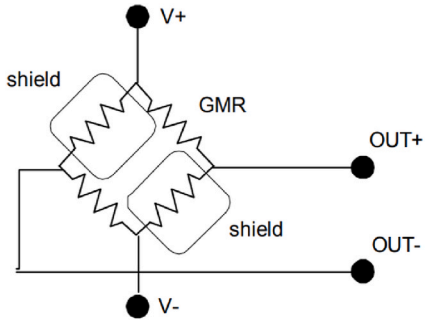

Fig. 2. Schematic diagram of the GMR sensor manufactured by NVE corporation [12].

with sensitivity of 7.75 mV/A. The use of a magnetic core improves the sensitivity of the sensor and suppresses the susceptibility to the electrical wire location and orientation in addition to enabling the adjustment of the sensitivity and the linear range by changing the gap of the magnetic core. However, it presents the same drawback as the previous sensor, due to the need of passing the conductor through a magnetic ring.

Finally, the magnetoelectric effect is being considered an attractive alternative for magnetic current sensing, with the potential to solve common problems in magnetic field sensors such as offset voltage, high dependence with temperature, need to signal amplification, nonlinearity and hysteresis. Castro et al. [7] reported a contactless direct current sensor based on the ME PVDF/Metglas composite and a solenoid that presents high linearity and sensitivity, $R^2 = 0.997$ and 476.5 mV/A, respectively. It is also a proximity sensor, as the prototype herein presented, so being considered the closest principle of operation and being compared in more details in the conclusion section.

Summarizing, this manuscript describes the development and experimental results of a prototype of ammeter that enables the measurement of direct currents with high resolution, in relation to the one presented by ammeters, clamp meters based on coils and Hall sensors. It is a proximity sensor based on two GMR sensors and precludes the need

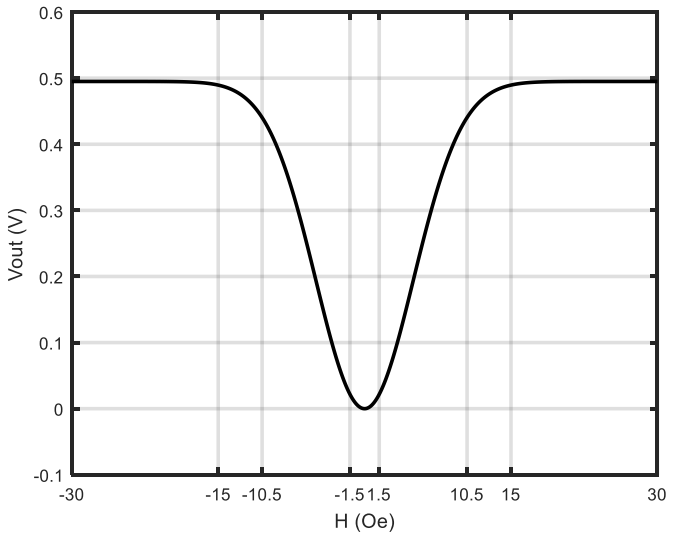

Fig. 3. GMR sensor output as a function of the external magnetic field.

for involving the conductor in a magnetic ring (as is the case of conventional clamp ammeters and of the majority of the above references). The proposed system was developed with the purpose of also estimating the distance between the instrument and the conductor, in specific applications, as in the case of conductors installed behind walls.

Next section describes GMR magnetometers and the present ammeter prototype design, including electronic circuit, hardware, software and inverse problem solution. Section 3 presents experimental results of the prototype, followed by a discussion and conclusions in Section 4.

2. Methods and procedures

2.1. GMR sensors

The giant magnetoresistance (GMR) is a phenomenon explained by quantum mechanics, characterized by a significant decrease in the electrical resistance, typically between 10 % and 80 %, which occurs when thin stacked multilayers of ferromagnetic and non-magnetic materials are exposed to a magnetic field. It was discovered in 1988 in independent works by physicists Albert Fert and Peter Grünberg, who in 2007 were awarded the Nobel Prize for Physics for their work [8–10].

The variation in the resistance of the multilayer occurs when the external magnetic field aligns the magnetic moments of the ferromagnetic layers, as shown in Fig. 1 [11]. In the absence of a magnetic field, the magnetizations of the ferromagnetic layers are antiparallel. With the application of a magnetic field H, greater than the saturation field H_S, the magnetizations are aligned in parallel, minimizing the electrical resistance of the multilayer. For magnetic fields smaller than the saturation field, the resistance is inversely proportional to the field. Also, it can be noticed that the reduction in the resistance is independent of the sign of the external magnetic field.

GMR sensors are typically configured as Wheatstone bridges to reduce temperature effects. GMR technology has low cost of production and small size. The disadvantages are high non-linearity, hysteresis and temperature influence [2].

This project is based on the GMR AAL002-02, manufactured by NVE Corporation [12]. The topology of the sensor is a Wheatstone half-bridge, having two magnetically shielded GMRs and two GMRs that are sensitive to the magnetic field, all in the same SOIC integrated circuit, as depicted in Fig. 2. Without the presence of an external magnetic field the bridge is balanced and the output of the bridge is zero. In the presence of an external magnetic field, the field-sensitive GMRs reduce their values according to the magnetic field in the direction of the sensor

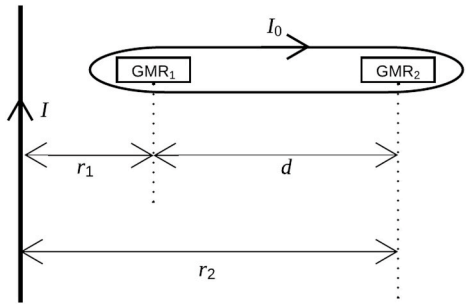

Fig. 4. Schematic diagram of the ammeter, showing the conductor with the current *I* to be measured, the two GMR sensors separated by a fixed distance *d* and the solenoid used to bias the sensors with a DC current Io. Both GMR sensors' sensitivity axes are aligned with the solenoid axis and orthogonal to the conductor.

axis, unbalancing the bridge and generating a differential voltage output.

The output signal of the bridge is directly proportional to the supply voltage/current, with a typical sensitivity of 3.5 mV/V/Oe (1 Oe = 1000/4π A/m) and a linear region ranging from 1.5 Oe to 10.5 Oe for the model AAL002-02. The nominal resistance is 5.5 kΩ and, when operating within the linear region, it presents a maximum linearity error of 2 % and a maximum hysteresis of 2 %. This differential voltage actually increases with the absolute value of the external magnetic field, as shown in Fig. 3 for a supply current of 2 mA (that yields a supply voltage of 11 V and a sensitivity of 38.5 mV/Oe).

2.2. Ammeter design

The goal of the ammeter under development is to measure electric currents in the range of ±20 A, passing through electrical conductors at close distance, from 1 cm up to 4 cm. An electric current passing through a wire generates a circular magnetic field around it that varies with the intensity of the current and with the distance from the conductor to the measuring point. By applying the Biot-Savart law to a straight conductor it is observed that the generated magnetic field *H* is given by

$$H = \frac{I}{500 r_1}, \tag{1}$$

where *I* is the electric current in amperes, r_1 is the distance between the conductor and the sensor in meters and *H* is the magnetic field in oersteds. Considering the values for current and distance above indicated, the maximum magnetic field to be measured by the GMR sensors is 4 Oe. For comparison purposes, the Earth's magnetic field is about 0.5 Oe.

If the distance r_1 is accurately known, it is easy to invert equation (1) and estimate the electric current from the magnetic field *H* that is measured by the GMR sensor. However, such is almost never the case and small differences in the estimated distance might yield large errors in the current. Also, in some applications the conductor might be installed within a wall, being the distance completely unknown.

Thus, the prototype is based on a configuration with two GMR sensors, with a known fixed distance *d* between them (0.9 cm), oriented so that the conductor whose current is to be estimated is positioned perpendicular to the plane where the GMRs are installed, in order to align the circumferential magnetic field generated by the current with the sensitivity axis of the sensors. This design was previously proposed

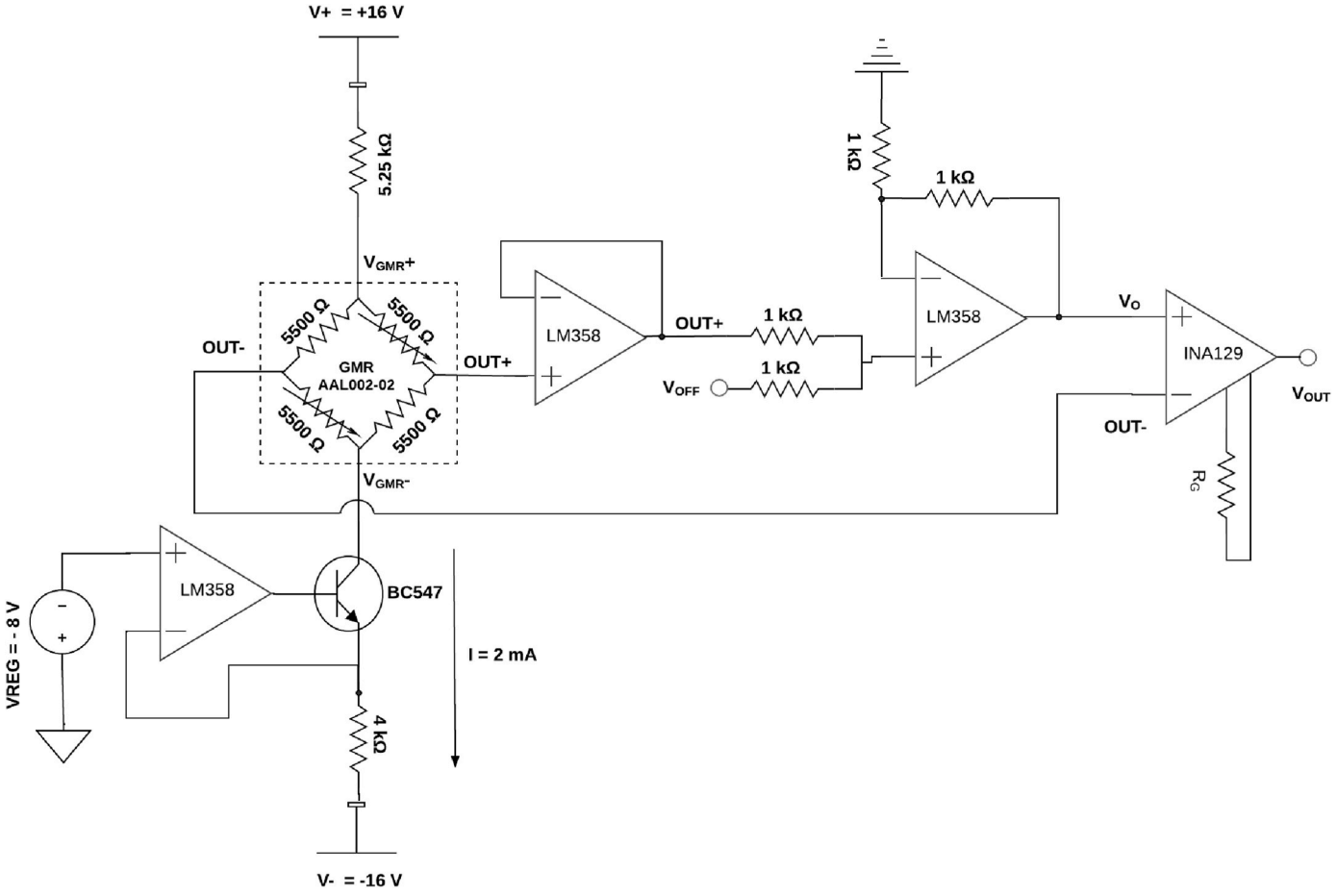

Fig. 5. Schematic diagram of the electronic conditioning circuit of GMR magnetometers.

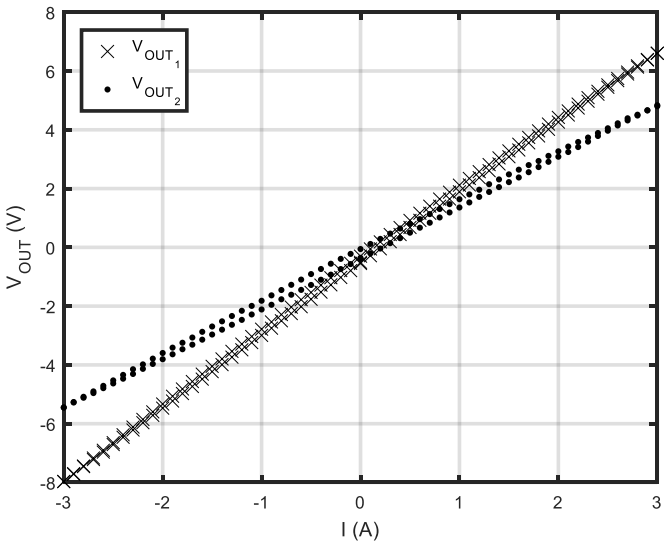

Fig. 6. Results of one experimental test for GMR_1 and GMR_2 with a distance $r_1 = 1$ cm.

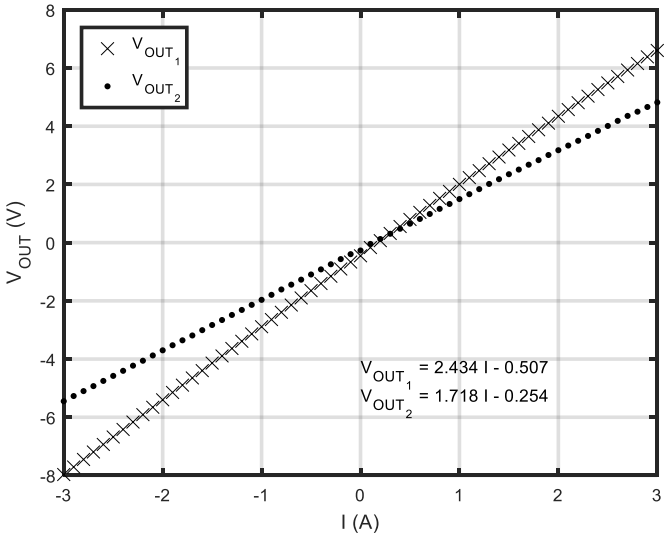

Fig. 7. Average values of the output voltages for each current value for GMR_1 and GMR_2 with a distance $r_1 = 1$ cm.

by Stefani Filho and Barbeta [13] and tested with a different GMR model and a separation of 3 cm. In this configuration, shown in Fig. 4, it is possible to estimate the electric current I without the need to know in advance the distances from the sensors to the conductor, and also to estimate these two distances r_1 and r_2.

As shown in Figs. 1 and 3, the GMR resistance varies only with the absolute value of the magnetic field and has a highly non-linear behavior close to $H = 0$ Oe. Therefore, it is necessary to apply a DC biasing magnetic field to make the sensors operate in their linear region, so that electrical currents in one direction increase the magnetic field applied to the sensor, whereas in the opposite direction they decrease that field. In previous versions of the ammeter [14–16], this biasing field was generated by a permanent magnet positioned close to the sensors, but this technique proved inefficient as it was difficult to find a position that polarized both sensors equally, and small variations in magnet positioning altered the biasing point.

The present design uses a solenoid with 60 turns (arranged in 3 layers of 20 turns), 3.5 cm length and 1.0 cm width, powered by a DC current $I_0 = 150$ mA and generating a biasing field of 6 Oe, so as to provide a

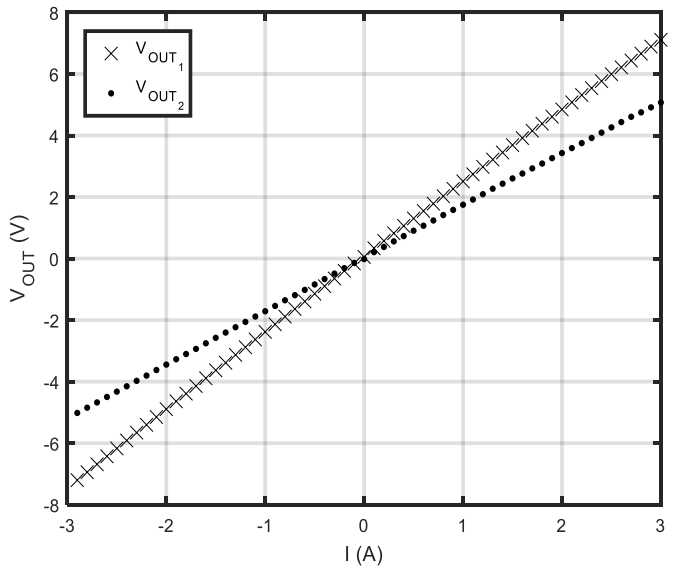

Fig. 8. Final result of the preprocessing for GMR1 and GMR2 with a distance $r_1 = 1$ cm.

dynamic range of ±4.5 Oe in the linear region with high accuracy and stability. Considering the typical sensitivity of 38.5 mV/Oe previously explained, this biasing field defines an operating point (offset) of 231 mV.

2.3. Electronic circuit

The electronic conditioning and reading circuit shown in Fig. 5 was designed and implemented in duplicate (one for each GMR sensor). The GMR sensor is shown in the dashed box and is modelled by 4 resistors of 5 kΩ in a Wheatstone bridge configuration. The potentiometers represent the unshielded GMR elements, thus varying with the external magnetic field.

The current source of 2 mA, based on the LM358 operational amplifier and the BC547 NPN transistor, feeds the GMR sensor through the terminals V_{GMR+} and V_{GMR-}. This configuration allows the cancellation of the common mode voltage in the output terminals OUT+ and OUT-, guaranteed by the voltage drop in the 5.25 kΩ resistor so that the voltage at terminal V_{GMR+} is 5.5 V. As this antisymmetrical bridge is always balanced, the current is split evenly, and the voltage at output terminal OUT-is always zero, while the voltage at output terminal OUT + varies around the operating point of 231 mV defined by the biasing magnetic field as previously described.

The null common mode voltage allows for a larger overall amplification by the following sections of the circuit, but there is still an offset voltage of approximately 231 mV that would prevent large gains. This offset voltage is removed by the non-inverting adder implemented by another LM358 operational amplifier, which adds the voltage of output terminal OUT+ (buffered through another LM358) to a negative offset voltage V_{OFF} (generated by a D/A converter, as explained in the next section), yielding the voltage V_O.

Finally, the instrumentation amplifier INA129 subtracts the voltage OUT-from the voltage V_O and applies a gain of 495 V/V for GMR_1 and 727 V/V for GMR_2, defined by the resistor R_G, yielding the overall output voltage V_{OUT}. The larger gain used for GMR_2 is due to the fact that, being 0.9 cm farther from the conductor, it is exposed to a smaller range of magnetic fields (−2 Oe to +2 Oe for the minimum r_1 distance).

2.4. Digital hardware and software

The analog hardware described in the previous section is complemented by a digital hardware comprising a National Instruments NI-

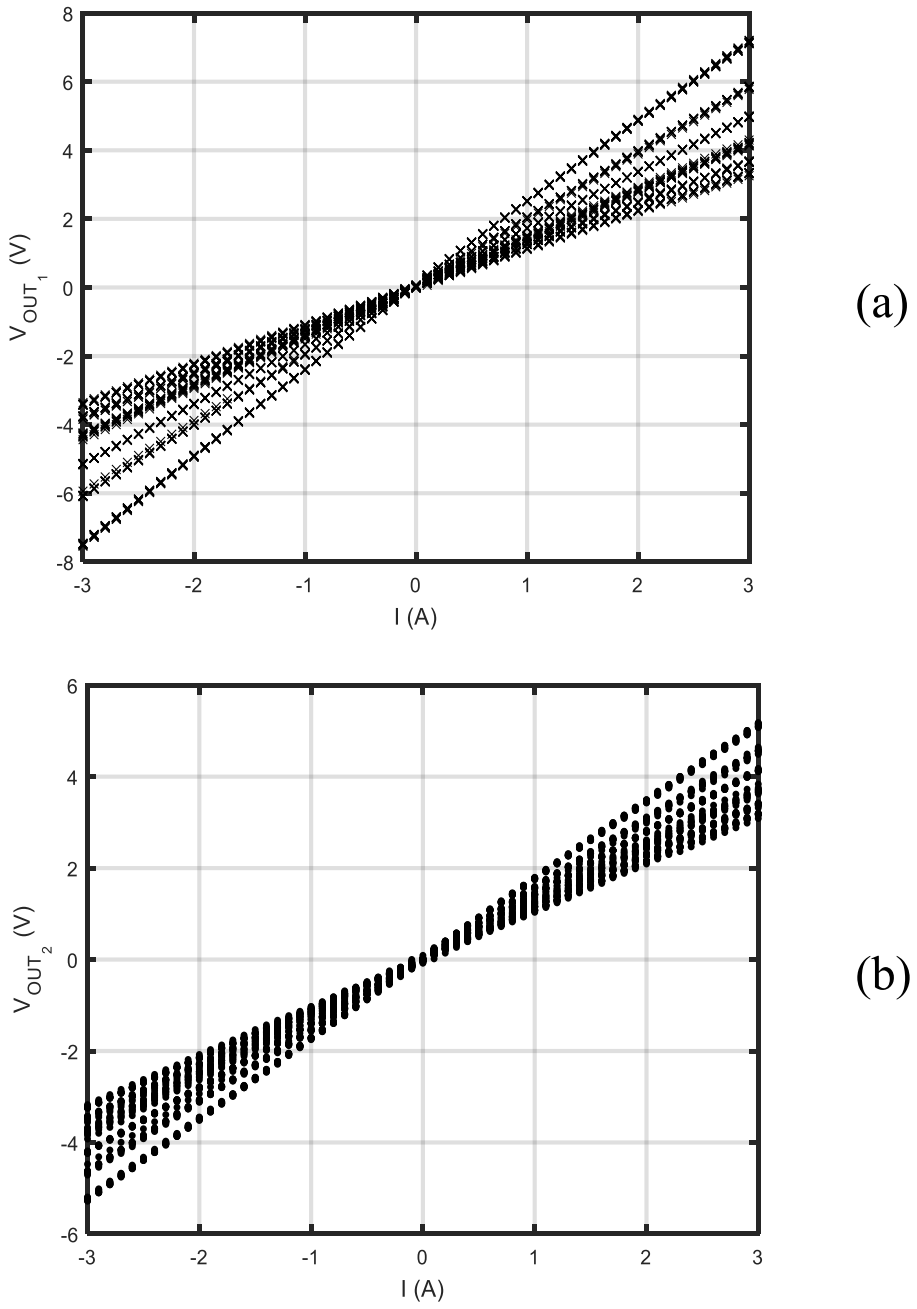

Fig. 9. Final result of the preprocessing for GMR_1 and GMR_2 for all 60 tests, with distances r_1 varying from 1.0 cm (largest inclination) to 2.0 cm (smallest inclination), in steps of 0.2 cm. (a) V_{OUT_1} and (b) V_{OUT_2}.

USB-6001 multifunction device and software developed in LabVIEW. Two analog input channels (14 bits resolution) of the device were used to acquire the two output voltages from the electronic conditioning circuit, each one related to one of the GMR sensors. In order to reduce the effects of noise and electromagnetic interference, each experimental sample consisted in the average value of a signal with 1 s length acquired with 5 kHz sampling frequency. The two analog output channels (14 bits resolution) were used to generate the offset compensation voltages (V_{OFF} in Fig. 5) for both GMR sensors.

The software also controls a Keysight B2962A 6.5 digits low noise current source through the USB interface, allowing the automation of the experimental tests described in Section 3. This digital source has 10 μA resolution, an error figure of ±(0.4 % + 7 mA) and a peak to peak noise lower than 60 μA in the frequency range of 0.1 Hz–10 Hz.

2.5. Signal processing (inverse problem)

As the objective is the development of an ammeter, it is necessary to solve the inverse problem, which is, given the two output voltages of the electronic conditioning system, measured by the data acquisition system, to estimate the electric current I flowing through the conductor, and the distance r_1.

As previously described, the magnetic fields perceived by both GMRs consist of two components: the magnetic field generated by the current I through the conductor and the biasing magnetic field generated by the solenoid so that the sensors operate in their linear range. However, since the offset voltage is removed by the non-inverting adder and theoretically does not contribute to the final output voltage, the magnetic field H perceived by the GMRs in this section will be considered (in oersteds) as

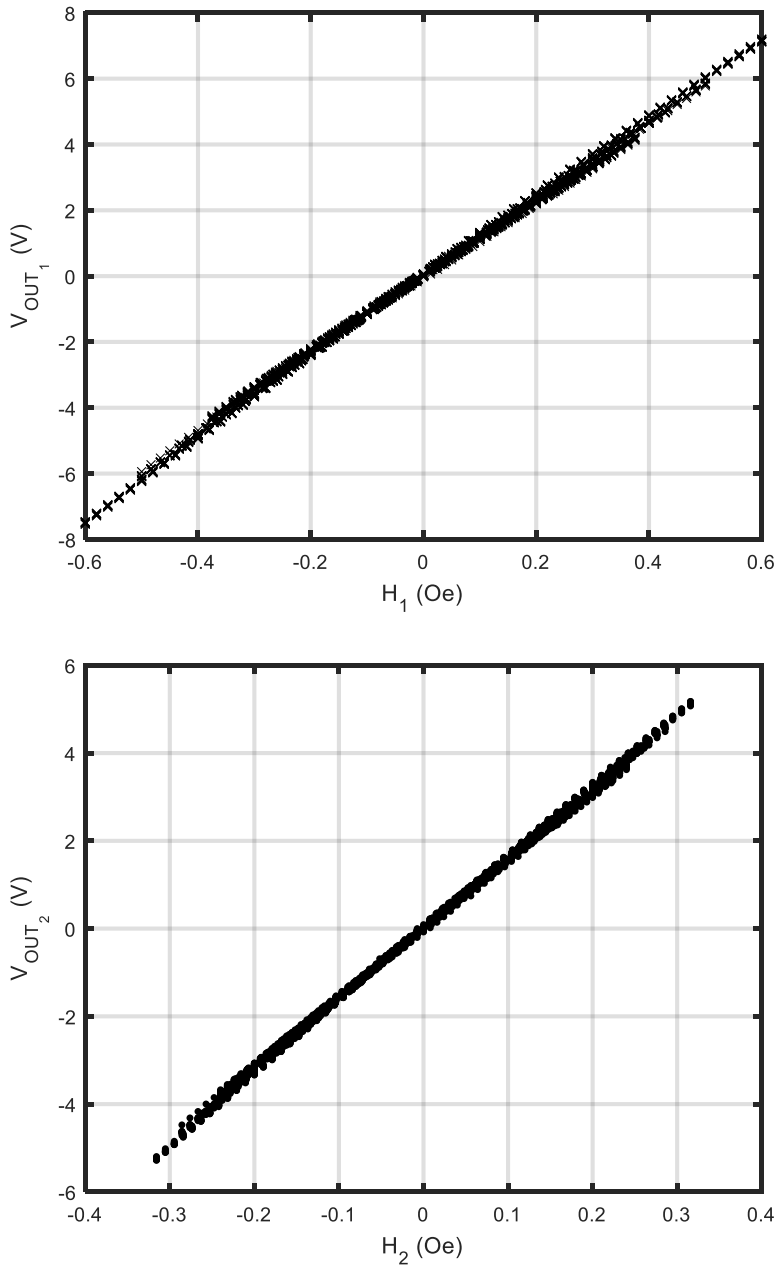

Fig. 10. Output voltages for both GMR electronic circuits plotted against the magnetic fields in each sensor. (a) V_{OUT_1} and (b) V_{OUT_2}.

Table 1
Coefficients corresponding to equations (6) and (7) for both GMR sensors.

Coefficients	Values
a_1	11.8049 V/Oe
a_2	15.9913 V/Oe
b_1	−18.725 μV
b_2	−19.793 μV

$$H_n = \frac{I}{500 r_n}, \tag{2}$$

where $n = 1$ or 2 to represent GMR_1 and GMR_2, respectively, and r_n is the distance between the conductor and each GMR, in meters. The two GMR sensors are separated by a fixed distance d, so that

$$r_2 = r_1 + d. \tag{3}$$

The GMR sensors output values are calculated by multiplying each magnetic field H_n by the sensitivity K_n and by adding an offset voltage V_{0_n} to account for effects of the electronic circuit components,

$$V_{GMR_n} = K_n H_n + V_{0_n}. \tag{4}$$

Finally, the output voltages of the conditioning circuit are given by the products of the voltages V_{GMR_n} by the respective gains provided by the instrumentation amplifiers (G_n), that is,

$$V_{OUT_n} = V_{GMR_n} G_n = [K_n H_n + V_{0_n}] G_n. \tag{5}$$

Equation (5) can be simplified as

$$V_{OUT_1} = a_1 . H_1 + b_1 \text{ and} \tag{6}$$

$$V_{OUT_2} = a_2 . H_2 + b_2 . \tag{7}$$

The coefficients a_1, a_2, b_1 and b_2, which define the linear

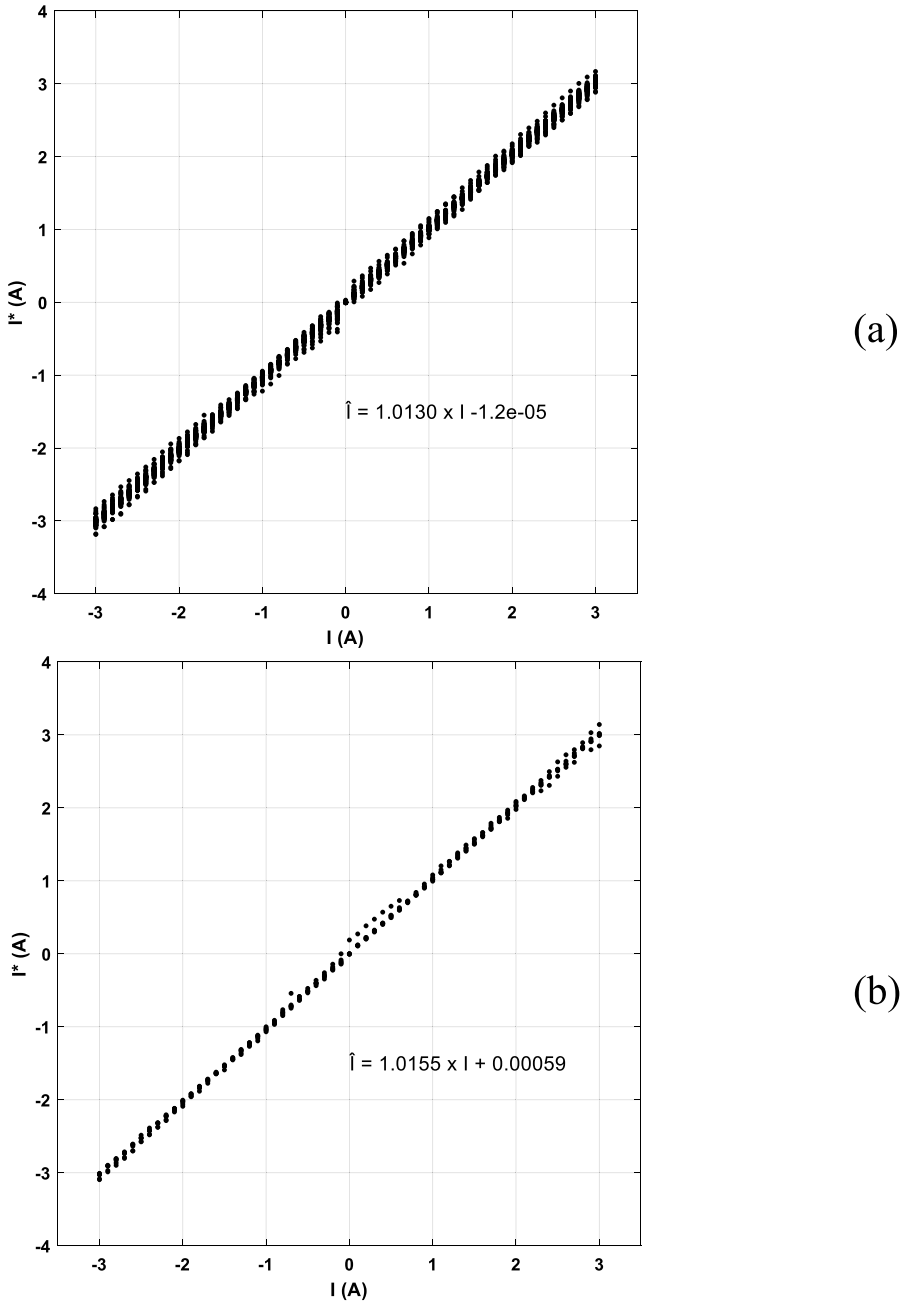

Fig. 11. Estimated currents (I^*) versus nominal currents (I) for (a) data used for the linear fitting that yielded the coefficients shown in Table 1. (b) Data not used for the linear fittings. The equations show the linear fits to the data in each graph.

relationships between the magnetic fields and the output voltages, can be estimated by a least squares fitting algorithm. Finally, by combining equation (2) with equations (6) and (7), the current I and the distance r_1 can be estimated from the output voltages V_{OUT_1} and V_{OUT_2} as

$$I^* = \frac{500 \cdot d \cdot (V_{OUT_2} - b_2) \cdot (V_{OUT_1} - b_1)}{a_2 \cdot (V_{OUT_1} - b_1) - a_1 \cdot (V_{OUT_2} - b_2)} \text{ and} \quad (8)$$

$$r_1^* = \frac{a_1}{500(V_{OUT_1} - b_1)} \cdot I^*. \quad (9)$$

3. Results

3.1. Data preprocessing

To observe the effect of the hysteresis and any other fluctuations, the tests were performed with currents varying between −3 A and 3 A in steps of 0.1 A, starting at 0 A, increasing up to 3 A, reducing down to −3 A and then closing the hysteresis cycle at 0 A. The tests used six different distances r_1, from 1.0 cm to 2.0 cm, with ten repetitions for each distance, totalling 60 tests. Fig. 6 presents one hysteresis cycle for the closest distance (1 cm), containing 123 data points.

The averages of the voltages for each current value are then calculated, yielding Fig. 7 with 61 data points. It can be noticed in Fig. 7 that the output voltages still present a sizeable offset of about 500 mV, even

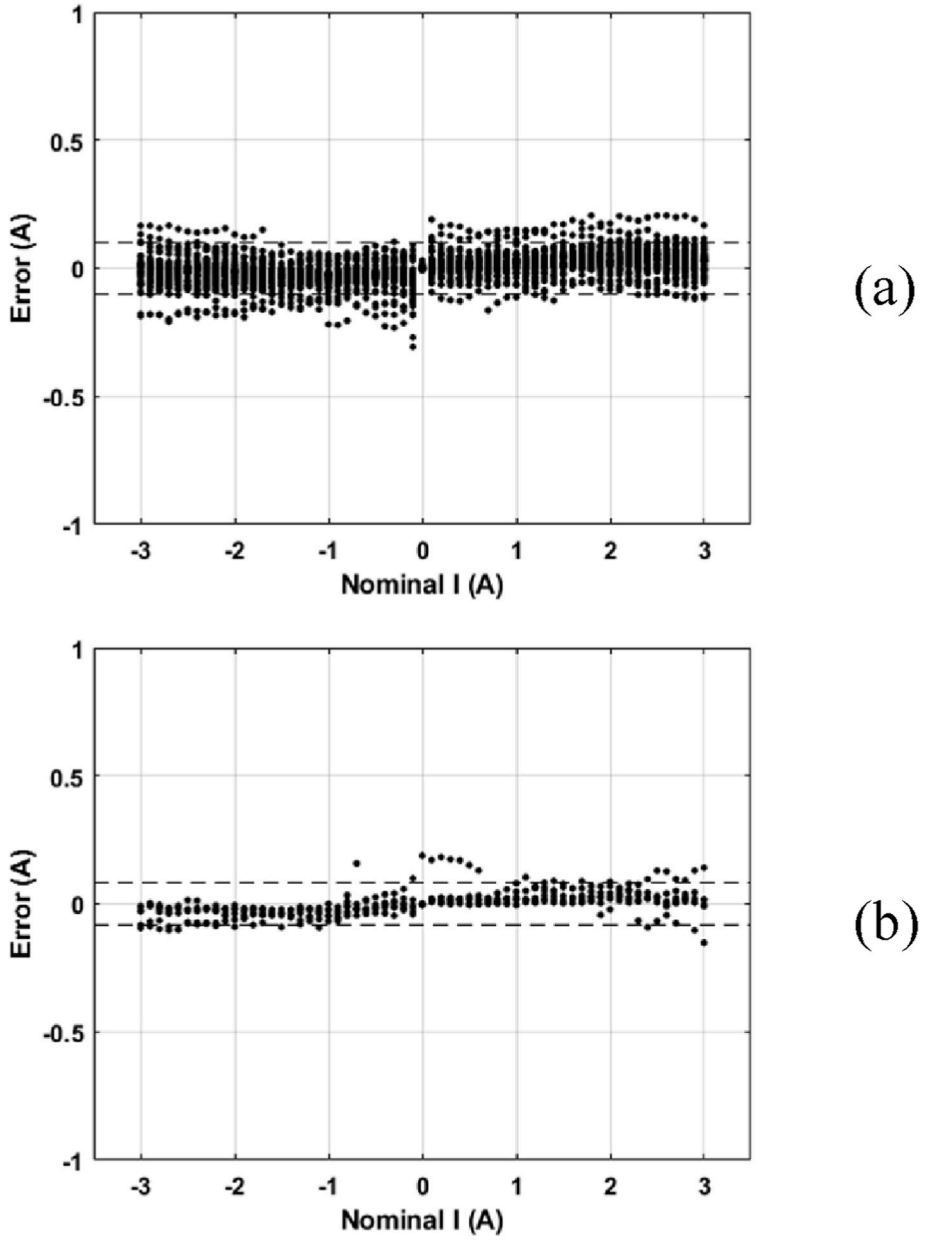

Fig. 12. Estimation errors (points) and uncertainties of the linear fits (dashed lines) for (a) data used for the linear fitting that yielded the coefficients shown in Table 1. (b) Data not used for the linear fittings.

after the cancellation by the circuit previously explained. This effect can be explained by the resolution of the 14 bits D/A converter, which for a full scale of 10 V is 0.610 mV. This value should be small enough, but it is multiplied by the instrumentation amplifier large gains, thus reaching the order of magnitude observed.

To correct this issue, the linear coefficient of the estimated trend lines for each test was subtracted from the output voltages. The results for $r_1 = 1.0$ cm can be seen in Fig. 8, containing the electrical current values and the respective output voltages.

The same procedure was repeated for all 60 tests, yielding a total of 3660 data points, shown in Fig. 9.

3.2. Inverse problem solution

The procedure described in section 2.5 was then applied to the data set shown in Fig. 9. Initially, the data were split in two sets, being one test for each distance separated from the rest, thus yielding a total of 9x61x6 = 3294 points to be used for the fitting. Then, the quantities H_1 and H_2 were calculated from the current and distance values according to equation (2), and Fig. 10 shows the respective output voltages plotted against these magnetic fields.

Linear fittings based on the data shown in Fig. 10 yielded the coefficients shown in Table 1, with corresponding R^2 values of 0.9986 and 0.9992, respectively. The application of equation (8) to estimate the electric currents from the output voltages generates the graphs shown in Fig. 11a for the data used for the linear fittings and in Fig. 11b for the data that was set aside for a final test of the inverse problem solution.

The expanded type An uncertainties of the linear fits, considering a 95.45 % level of confidence, can be calculated from the errors between the estimated currents (I^*) and the linear fit ($\hat{I}$) as

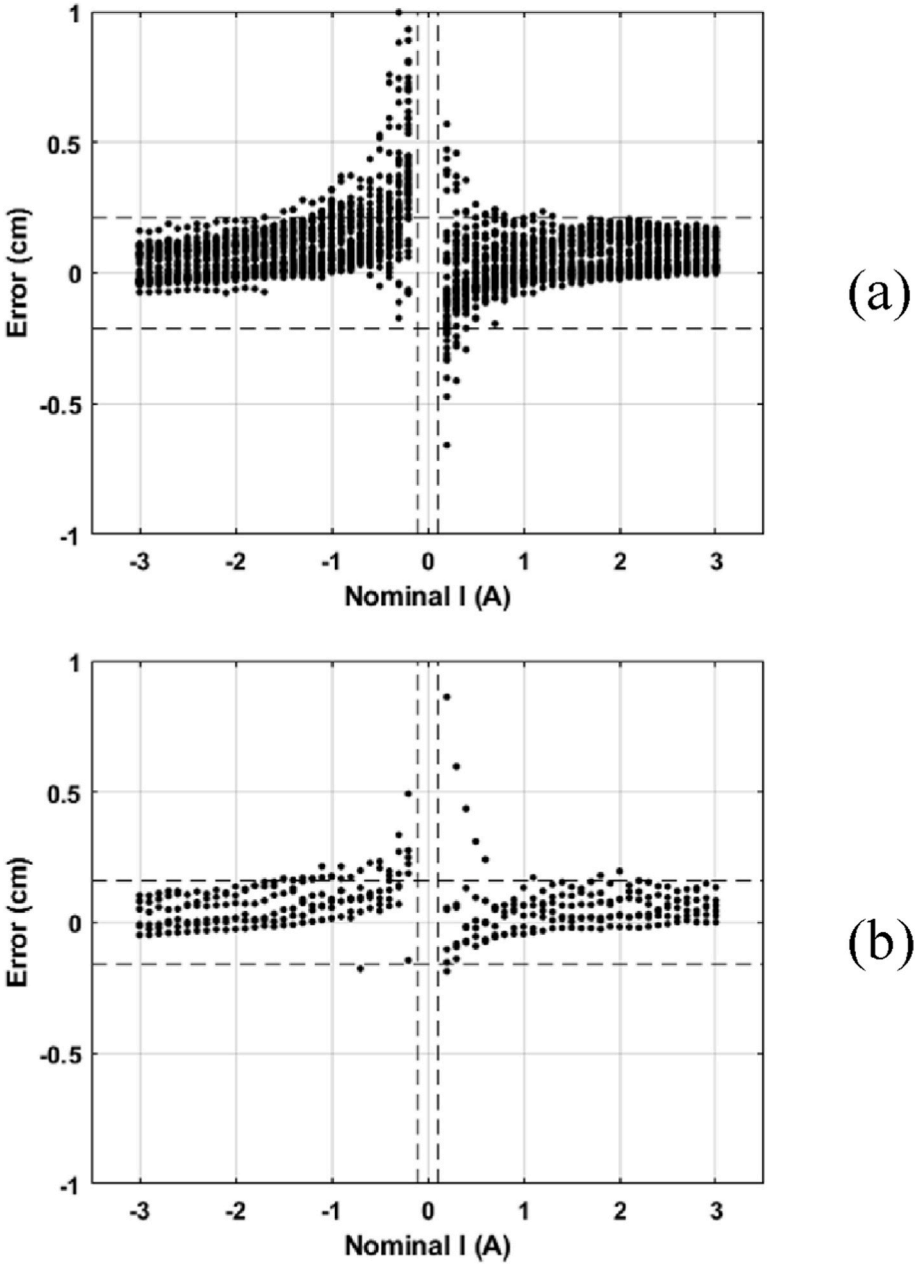

Fig. 13. Estimation errors (points), current uncertainty of the linear fit (vertical dashed lines) and distance uncertainty of the linear fit (horizontal dashed lines) for (a) data used for the linear fitting that yielded the coefficients shown in Table 1. (b) Data not used for the linear fittings, in both cases excluding the points for which $I > u_I$.

$$u_I = 2 \times \sqrt{\frac{\sum_{k=1}^{N} \left(I_k^* - \hat{I}_k\right)^2}{N-2}}. \quad (10)$$

N being 3294 and 366 for each data set, respectively. Fig. 12 presents the estimation errors corresponding to the data shown in Fig. 11, which yielded expanded type An uncertainties of the linear fits of 102.6 mA and 83.9 mA, respectively, also shown in Fig. 12.

As for the estimation of the distance r_1 from the conductor to the first GMR, observing equations (2), (3) and (9) it can be seen that (i) there is an indetermination for null currents, as no magnetic field would be generated and it would make no sense to estimate a distance and (ii) the error in the distance r_1 is highly dependent on the error in the estimated current I^*. Considering the uncertainty of the linear fit for estimated current I^* previously calculated, it can be defined that the distances can be estimated only for the cases where the absolute value of the estimated current is larger than the uncertainty. Thus, Fig. 13 presents the estimation errors for the distance r_1 corresponding to the two previous sets of data, but excluding the cases in which the nominal current was smaller than u_I. The uncertainties of the linear fits for the distances were calculated, similarly as the procedure used for the currents, as 0.21 cm and 0.16 cm, respectively, also shown in Fig. 13.

Finally, Fig. 14 presents the actual estimated distances corresponding to the cases shown in Fig. 13.

4. Conclusions

Electrical current measurement is important in many industry sectors residential applications and several measurement methods have been developed to meet these needs. GMR magnetometers present a low-

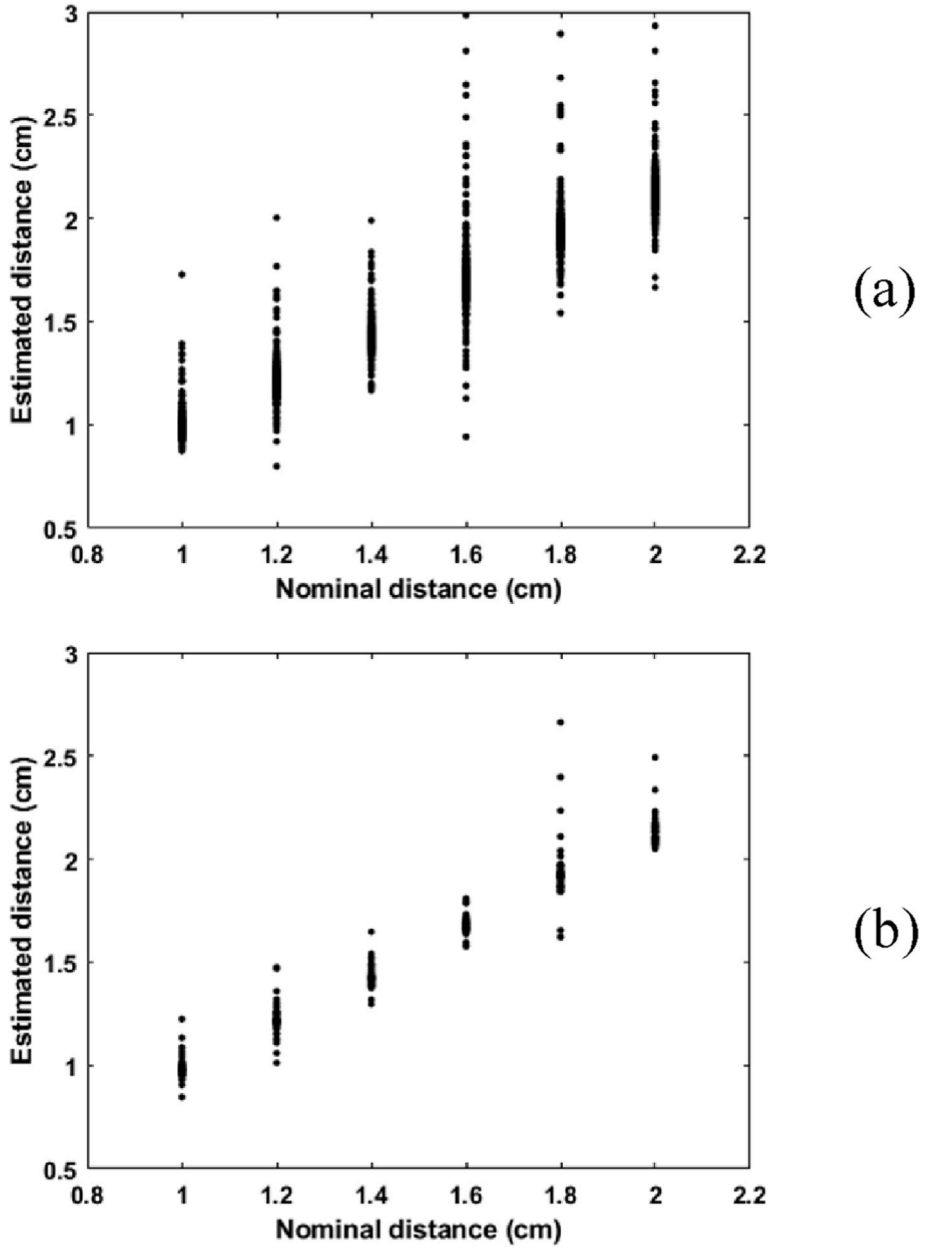

Fig. 14. Estimated distances versus nominal distances for (a) data used for the linear fitting that yielded the coefficients shown in Table 1. (b) Data not used for the linear fittings, in both cases excluding the points for which $I > u_I$.

cost, high-sensitivity solution for the development of an ammeter, capable of measuring direct currents in a non-invasive way.

This manuscript presented a prototype of a proximity contactless ammeter aimed at residential and industrial direct current measurements, based on commercial GMR magnetometers, being an evolution of prior developments of the same principle [14–16] and inspired in the design proposed by Ref. [13]. The ammeter, besides being contactless (and thus not requiring the interruption of the electric circuit where the current is to be measured and increasing user safety), needs only to be approximated to the conductor, differently from the traditional clamp ammeters that need the conductor to pass through a solenoid or a magnetic ring. Further tests are needed in order to evaluate the robustness of the prototype in relation to magnetic interference and temperature, before it can be evolved into a commercial ammeter.

Considering the closest distance tested only (1 cm), the data shown in Fig. 8 can be used to calculate an average sensitivity of 2.076 V/A, more than 4 times larger than the value estimated for the ME-based prototype developed by Castro et al. [7].

The results obtained yielded an expanded uncertainty of about 100 mA, considering only the type An uncertainty component, with a confidence level of 95.45 %. The range used for the test was limited by the available experimental apparatus to ±3 A, so the expanded uncertainty corresponds to 1.7 % of the full measurement range.

Nevertheless, the high linearity shown in Figs. 10 and 11 indicate that the range can be easily increased (by reducing the instrumentation amplifier gains in order to avoid saturation), being limited in principle only by the linear range of the GMR. In fact, the present experimental results covered a magnetic induction range of ±0.6 Oe (Fig. 10a), while the GMR sensors have been biased so as to offer a linear range of ±4.5 Oe, so there is a factor of 7.5 for potential increasing in the current up to the range of approximately ±20 A. Also, Figs. 12 and 13 show that the errors are stable as the current increases, so it would be reasonable to consider that the uncertainty would remain around 100 mA, or even reduce, as the range increases, which would reduce its percent value to

about 0.25 % considering the full range ±20 A.

The manuscript by Castro et al. [7] did not present measurement uncertainty figures, so a direct comparison of this aspect is not possible, but the linearity shown in Fig. 10 is even higher than the figure reported in this reference ($R^2 = 0.997$).

Aiming at upgrading the prototype, in order to reduce the measurement uncertainties, make it more compact and portable, the following analyses and studies are proposed as future work:

- In order to obtain a more accurate estimate of sensitivity, compared to that obtained experimentally, the GMR sensors could be previously characterized using a Helmholtz coil coupled to a calibrated current source;
- The use of the solenoid for the polarization of the GMRs has proven to be more practical and precise in relation to the use of permanent magnets. However, some improvements can still be implemented, such as increasing the number of turns, consequently decreasing the required current and including a dedicated current source to power the solenoid in the PCB;
- Another approach to further increase the current range is to include a feedback loop that automatically adjusts the biasing DC current I_0 in order to keep the GMR sensors within their linear ranges even for larger currents, similarly to the scheme described in a previous work [17].
- In principle, the present electronic circuit should already allow the measurement of low frequency alternating currents. Thus, simulations and tests should be performed with alternating currents at the typical industrial frequencies (50 Hz and 60 Hz) and with direct currents of higher intensity, varying from 0 to 20 A; and
- The prototype should be metrologically characterized in an accredited calibration laboratory, in order to determine the static and dynamic characteristics that indicate its quality, such as sensitivity and linearity, in addition to comparing these results with commercial ammeters.

Acknowledgments

The authors thank for the financial support provided by the Brazilian funding agencies CNPq, CAPES, FINEP, and FAPERJ. This study was financed in part by the Coordenação de Aperfeiçoamento de Pessoal de Nível Superior, Brasil (CAPES), Finance Code 001.

References

[1] P. Ripka, Electric current sensors: a review, Meas. Sci. Technol. 21 (11) (2010) 112001, https://doi.org/10.1088/0957-0233/21/11/112001.
[2] S. Ziegler, R.C. Woodward, H.H. Iu, L.J. Borle, Current sensing techniques: a review, IEEE Sensor. J. 9 (4) (2009) 354–376, https://doi.org/10.1109/JSEN.2009.2013914.
[3] J. Sánchez, D. Ramírez, J. Amaral, S. Cardoso, P.P. Freitas, Electrical ammeter based on spin-valve sensor, Rev. Sci. Instrum. 83 (10) (2012) 105113, https://doi.org/10.1063/1.4759020.
[4] P. Pai, L. Chen, F.K. Chowdhury, M. Tabib-Azar, Non-intrusive electric power sensors for smart grid, in: 2012 IEEE Sensors Conference, Taipei, Taiwan, October 2012, pp. 28–31, https://doi.org/10.1109/ICSENS.2012.6411383.
[5] Y. Xiaoguang, L. Hang, W. Yuanyuan, W. Youhua, D. Guoya, Z. Zhenghan, A giant magneto resistive (GMR) effect based current sensor with a toroidal magnetic core as flux concentrator and closed-loop configuration, IEEE Trans. Appl. Supercond. 24 (3) (2012) 9000305, https://doi.org/10.1109/TASC.2013.2286396.
[6] O. Yong, H. Jinliang, H. Jun, Z. Gen, W. Zhongxu, S.X. Wang, Contactless current sensors based on magnetic tunnel junction for smart grid applications, IEEE Trans. Magn. 51 (11) (2015) 4004904, https://doi.org/10.1109/TMAG.2015.2446332.
[7] N. Castro, S. Reis, M.P. Silva, V. Correia, S. Lanceros-Mendez, P. Martins, Development of a contactless DC current sensor with high linearity and sensitivity based on the magnetoelectric effect, Smart Mater. Struct. 27 (6) (2018) 065012, https://doi.org/10.1088/1361-665X/aab969.
[8] M.N. Baibich, J.M. Broto, A. Fert, F. Nguyen, F. Petroff, P. Eitenne, O. Creuzet, A. Friederich, J. Chazelas, Giant magnetoresistance of (001)Fe/(001)Cr magnetic superlattices, Phys. Rev. Lett. 61 (21) (1988) 2472, https://doi.org/10.1103/PhysRevLett.61.2472.
[9] G. Binasch, P. Grünberg, F. Saurenbach, W. Zinn, Enhanced magnetoresistance in layered magnetic structures with antiferromagnetic interlayer exchange, Phys. Rev. B 39 (1) (1989) 4828, https://doi.org/10.1103/PhysRevB.39.4828.
[10] L. Chang, M. Wang, L. Liu, S. Luo, P. A. Xiao, A brief introduction to giant magnetoresistance. Online [accessed 24 March 2024] https://arxiv.org/abs/1412.7691.
[11] I. Ennen, D. Kappe, T. Rempel, C. Glenske, A. Hütten, Giant magnetoresistance: basic concepts, microstructure, magnetic interactions and applications, Sensors 16 (6) (2016) 904, https://doi.org/10.3390/s16060904.
[12] NVE Corporation, AA and AB-Series Analog Sensors. Online [accessed 24 March 2024] https://www.nve.com/analogSensors.php.
[13] C.L. Stefani Filho, V.B. Barbeta, Amperímetro DC não invasivo utilizando sensor GMR, Revista Pesquisa & Tecnologia FEI 21 (2001) 14–18.
[14] M.C. Carvalho, C.S. Neves, C.R.H. Barbosa, E.C. Silva, L.A.P. Gusmão, Contactless ammeter based on GMR sensors, in: VIII Brazilian Metrology Conference, Bento Gonçalves, Brazil, 29 November – 2, December 2015. Online, https://iopscience.iop.org/article/10.1088/1742-6596/733/1/011001. (Accessed 24 March 2024).
[15] C.S. Neves, D.P. Magalhães, C.R.H. Barbosa, GMR sensors and neural networks applied to the contactless measurement of direct electrical currents, J. Physics Conf. Series 975 (2018) 012070, https://doi.org/10.1088/1742-6596/975/1/012070.
[16] C.S. Neves, D.P. Magalhães, C.R.H. Barbosa, E.C. Oliveira, A contactless ammeter based on GMR magnetometers, J. Physics Conf. Series 1044 (2018) 012001, https://doi.org/10.1088/1742-6596/1044/1/012001.
[17] T.Y. Poon, N.C.F. Tse, R.W.H. Lau, Extending the GMR current measurement range with a counteracting magnetic field, Sensors 13 (6) (2013) 8042–8059, https://doi.org/10.3390/s130608042.

Camila Schuina Neves[a], Carlos Roberto Hall Barbosa[a,*], Eduardo Costa da Silva[b], Daniel Prado de Magalhães[b], Luiz Antonio Pereira Gusmão[b]

[a] *Postgraduate Programme in Metrology, Pontifical Catholic University of Rio de Janeiro, Rio de Janeiro, Brazil*

[b] *Electrical Engineering Department, Pontifical Catholic University of Rio de Janeiro, Rio de Janeiro, Brazil*

[*] Corresponding author.

E-mail addresses: camila_schuina@hotmail.com (C.S. Neves), hall@puc-rio.br (C.R. Hall Barbosa), edusilva@ele.puc-rio.br (E. Costa da Silva), danielpmagalhaes@gmail.com (D. Prado de Magalhães), lgusmao@ele.puc-rio.br (L.A. Pereira Gusmão).